Supercapacitor-Based Inertia Support Control Strategy for Generator Units in Microgrids

Jianning Wang
Logistic Engineering College, Shanghai Marine University, Shanghai 201306, China
Corresponding author: Jianning Wang (e-mail: lg-wjn@163.com)

ABSTRACT With the increasing penetration of inverter-based renewable energy sources, low-inertia microgrids are more vulnerable to severe frequency excursions, high rates of change of frequency (RoCoF), and fast electromagnetic transients under sudden disturbances. This study proposes a coordinated supercapacitor-based virtual inertia support strategy in which active power is injected proportionally to RoCoF while voltage and energy constraints are strictly enforced. A microgrid model including three 2 MW synchronous generators, two coordinated 50 F supercapacitor units, photovoltaic generation, and frequency-dependent dynamic loads is established in MATLAB/Simulink. To reduce sensitivity to measurement noise in derivative-based control, a first-order low-pass filter is incorporated into the control loop. The proposed strategy is evaluated under representative scenarios, including a 20% load step, a 2 MW generator trip, and $\pm$ 15% band-limited stochastic photovoltaic fluctuations. Compared with the no-supercapacitor baseline, the coordinated multi-supercapacitor strategy reduces the maximum frequency deviation from 0.61 $\pm$ 0.02 Hz to 0.32 $\pm$ 0.01 Hz and shortens settling time from 14.8 $\pm$ 0.5 s to 8.7 $\pm$ 0.3 s under the 20% load-step condition. The coordinated control also reduces the peak power burden on each unit and improves state-of-energy balance, indicating improved short-term frequency regulation.

INDEX TERMS microgrid,supercapacitor,virtual inertia,frequency stability,electromagnetic transients

I. INTRODUCTION

THE rapid integration of renewable energy sources (RES), such as photovoltaic (PV) and wind power, into modern microgrids [1] has fundamentally altered the dynamic characteristics of power systems [2]. The replacement of conventional synchronous generators with inverter-based resources significantly reduces system-wide rotational inertia. As a result, low-inertia microgrids are increasingly susceptible to severe frequency excursions and high rates of change of frequency (RoCoF) during common disturbances, including abrupt load variations, generator tripping, or intermittent renewable generation [3-5]. These transient frequency deviations can not only compromise power quality but also impose mechanical stress on conventional equipment and sensitive loads, highlighting the need for rapid and reliable frequency support.

Conventional frequency regulation relies on the kinetic energy stored in rotating masses of synchronous generators. While Battery Energy Storage Systems (BESS) are widely deployed for primary frequency control, their capability to emulate instantaneous inertia is limited. High-power electronics enable rapid response, but frequent high-magnitude injections during sub-second intervals can accelerate electrochemical degradation and thermal stress, significantly reducing operational lifespan [6]. Recent studies have attempted to address these challenges using SCs, but many do not consider multi-unit coordination under strict voltage and energy constraints or the effect of measurement noise on derivative-based control loops [7,8].

Supercapacitors (SCs) have emerged as an effective solution for virtual inertia emulation due to their high power density, rapid charge/discharge capability, and long cycle life (typically >500,000 cycles) [9-11]. SCs can bridge the gap between millisecond-scale electromagnetic transients and the slower mechanical response of traditional governors, making them suitable for low-inertia microgrids. Recent studies have investigated SC-based frequency support, RoCoF-based virtual inertia control, and energy-storage-assisted frequency regulation in renewable-dominated microgrids and microgrid clusters [12-15], showing that these strategies can effectively improve transient stability and frequency response. However, existing studies still tend to overlook the interaction between fast derivative-based control and measurement noise, or fail to provide effective multi-unit energy coordination under strict voltage and energy constraints.

To address these gaps, this study proposes a comprehensive SC-based inertia support strategy emphasizing both dynamic performance and hardware safety, with the following key contributions:

1. Dynamic Modeling: A high-fidelity microgrid model is developed, incorporating three 2 MW synchronous generators and a coordinated SC array (2 × 50 F) with an RLC-equivalent circuit. This modeling captures realistic millisecond-scale transients and provides a clearly parameterized simulation platform for evaluating short-term frequency-support performance and potential hardware-in-the-loop (HIL) validation.
2. Noise-Resilient Control: A RoCoF-based virtual inertia control law is designed with an integrated first-order low-pass filter (LPF) to mitigate the impact of sensing noise, ensuring smooth and stable SC power injection even under stochastic load and PV fluctuations.
3. Coordinated Energy Management: An adaptive power-sharing law based on the State-of-Energy (SoE) is implemented to ensure balanced utilization across multiple SC units. The method strictly enforces the energy boundary of each SC unit and the 600–900 V voltage window, reducing the risk of inverter overcurrent and helping reduce long-term operational stress.
4. Validation and Sensitivity: The strategy is rigorously validated against extreme contingencies, including a 2 MW DG trip and ±15% PV fluctuations. Sensitivity analysis further confirms stable performance under ±20% variations in inertia gain and SC capacitance.

By providing a reproducible methodology with mathematically consistent parameters, this study offers a practical basis for enhancing the resilience, stability, and reliability of modern low-inertia power systems.

II. MICROGRID SYSTEM MODELING

This section presents a detailed modeling framework for the studied microgrid, incorporating distributed generation units, supercapacitor energy storage, frequency-dependent loads, and stochastic renewable generation. The model is intended to support dynamic analysis and stability assessment under representative operating conditions, and it also provides a basis for future hardware-in-the-loop (HIL) validation.

A. MICROGRID TOPOLOGY AND OPERATING MODES

The microgrid architecture shown in Figure 1 consists of the following key components:

- Distributed Generation Units (DGs): Three synchronous generators (SGs), each rated at 2 MW, provide the primary power supply and the physical rotational inertia required for frequency stabilization.
- Supercapacitor Energy Storage (SC): Two high-power supercapacitor units are deployed to provide fast-response virtual inertia support. Each unit has an equivalent capacitance of 50 F, with an operating voltage range of 600–900 V, representing a realistic aggregated module configuration composed of multiple commercial supercapacitor cells.

The maximum available energy of each SC unit is calculated as

$$E_{\max} = \frac{1}{2} C \left(V_{\max}^2 - V_{\min}^2 \right) \tag{1}$$

- Loads: The load model consists of a combination of static loads (2–3 MW) and frequency-dependent dynamic loads, represented as

$$P_L = P_{L0} \left[1 + K_f (f - f_0) \right] \tag{2}$$

where $K_f = 0.05$ pu/Hz is the load-frequency sensitivity coefficient. To emulate realistic operating conditions, stochastic load variations of ±5% are introduced using Gaussian white noise.

- Renewable Energy Sources (RES): Photovoltaic (PV) arrays are modeled as variable power injections with ±15% band-limited stochastic fluctuations. The Gaussian random sequences are processed through a first-order low-pass filter with a correlation time of 1 s before being injected into the simulation model, thereby avoiding unrealistic high-frequency PV power variations caused by unbounded white noise.

The system can operate in both grid-connected and islanded modes, enabling comprehensive evaluation of the proposed control strategy under different operating scenarios. This topology facilitates the investigation of SC-based virtual inertia support under both normal and extreme disturbances, providing insights into system stability, robustness, and dynamic performance.

B. DISTRIBUTED GENERATION UNIT MODELING

Each DG unit is represented using the classical swing equation to capture rotor dynamics:

$$\frac{2H_i}{\omega_s} \frac{d\Delta\omega_i}{dt} = P_{m,i} - P_{e,i} - D_i(\omega_i - \omega_s) \tag{3}$$

where H_i is the inertia constant, ω_i and ω_s are rotor and synchronous angular speeds, $P_{m,i}$ and $P_{e,i}$ are mechanical and electrical powers, and D_i is the damping coefficient.

The typical parameters for each DG unit used in the simulations are summarized in Table 1, which shows rated power, inertia, damping, and droop coefficients. These values are chosen to reflect realistic synchronous generators commonly deployed in industrial microgrids, providing both physical inertia and frequency regulation capability.

TABLE 1. Typical Parameters per DG Unit

Parameter	Symbol	Value
Rated Power	P_{rated}	2 MW
Inertia Constant	H	4 s
Damping	D	0.02 pu
Droop Coefficient	R	5%

Note in text: The parameters in Table 1 are used to compute the equivalent system inertia H_{eq} and to simulate

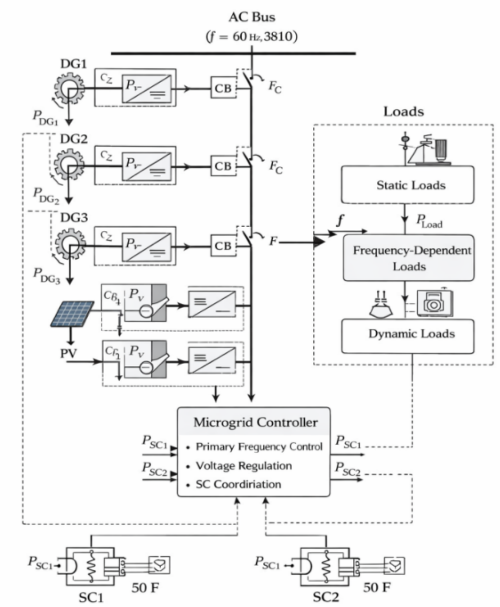

FIGURE 1. Architecture of the studied microgrid including three synchronous generators, photovoltaic generation, coordinated supercapacitor storage units, and dynamic loads connected to a common AC bus

the frequency response under load-step and contingency conditions.

C. LOAD MODELING

The load is modeled as a combination of static and frequency-dependent components:

$$P_L = P_{L0} + K_f P_{L0}(\omega - \omega_s) \tag{4}$$

where P_{L0} is the constant static load and $K_f = 0.05$ pu/Hz is the load-frequency sensitivity coefficient. To emulate realistic operating conditions while avoiding unrealistic high-frequency power injections, stochastic load variations were generated as Gaussian random sequences and then processed through a first-order low-pass filter before being applied to the load model. The variation amplitude was limited within $\pm 5\%$, and the correlation time was set to 0.2 s. In addition, each simulation scenario was repeated five times, and the results are reported as mean $\pm$ standard deviation to improve statistical robustness and reproducibility. This load representation enables evaluation of SC control performance under stochastic but band-limited operating disturbances.

D. SUPERCAPACITOR (SC) ENERGY STORAGE MODELING

Each SC unit is modeled as a series RLC circuit, and its voltage and energy constraints are explicitly enforced to ensure safe operation. The adopted SC parameters, including capacitance, voltage range, series resistance, and maximum available energy, are summarized in Table 2.

The values in Table 2 are selected to represent commercially available SC units and the operational constraints considered in this study. These parameters directly affect the SC's ability to provide rapid virtual inertia support and to accommodate stochastic load and PV fluctuations without exceeding safe operating limits. Small random variations (~$\pm$0.5–1%) are introduced in voltage and current to emulate realistic transient behavior.

TABLE 2. Corrected SC Parameters

Parameter	Symbol	Value
Capacitance	C	50 F
Voltage Range	V_{SC}	600–900 V
Series Resistance	R_{SC}	0.01 Ω
Maximum Energy	$E_{\max}$	11.25 MJ

Note in text: The parameters in Table 2 are used in the state-space frequency model to calculate SC power injection P_{SC} and to ensure that multi-unit SoE coordination remains within physical constraints.

E. MICROGRID FREQUENCY DYNAMICS

The equivalent system frequency deviation is governed by the combined inertia of the DG units and the SC-based virtual inertia support:

$$\frac{d\omega_{eq}}{dt} = \frac{1}{2H_{eq}}\left(\sum_i P_{m,i} + \sum_k P_{SC,k} - \sum_j P_{L,j} - D_{eq}(\omega_{eq} - \omega_s)\right) \quad (5)$$

where H_{eq} denotes the total equivalent inertia, $P_{m,i}$ is the mechanical power of DG unit i (MW), $P_{SC,k}$ is the power injected by SC unit k (MW), $P_{L,j}$ is the load power of load component j (MW), D_{eq} is the equivalent load damping coefficient, and ω_{eq} and ω_s are the equivalent system angular speed and synchronous angular speed, respectively.

To emulate realistic operating conditions, small stochastic perturbations (~±0.01–0.02 Hz in $\Delta\omega$) are introduced into the frequency signal. These perturbations are used to assess the robustness of the proposed control strategy under measurement variations and practical operating uncertainty.

III. PROPOSED SC-BASED INERTIA SUPPORT CONTROL STRATEGY

This section presents the proposed SC-based virtual inertia control strategy, with emphasis on inertia emulation, energy management, and multi-unit coordination under practical operating constraints.

A. CONTROL PRINCIPLE AND TRANSFER FUNCTION

The primary objective of the proposed strategy is to emulate the inertial response of synchronous generators. Unlike conventional batteries, SCs provide high power density and fast charge/discharge capability, enabling rapid transient active power injection in response to the Rate of Change of Frequency (RoCoF). RoCoF-based virtual inertia control has been widely adopted to improve transient frequency support in inverter-dominated systems [16,17].

To mitigate the high-frequency noise associated with derivative calculations, a first-order low-pass filter (LPF) is incorporated into the control loop. The SC power injection in the s-domain is expressed as

$$P_{SC}(s) = -\frac{K_H s}{\tau s + 1}\Delta\omega(s) \quad (6)$$

where $P_{SC}(s)$ denotes the SC power injection (MW), K_H is the virtual inertia gain (MW·s/rad), τ is the filter time constant (0.01–0.05 s), and $\Delta\omega(s)$ is the system frequency deviation (rad/s).

The LPF suppresses high-frequency oscillations and helps ensure smooth SC power injection under noisy measurements, thereby improving control robustness. The overall implementation framework of the proposed RoCoF-based virtual inertia control strategy is illustrated in Figure 2.

B. OPERATIONAL ENVELOPE AND CONSTRAINT ENFORCEMENT

To protect hardware and prevent accelerated SC degradation, dynamic operational constraints are enforced:

1) Voltage Boundary

$$V_{\min} \le V_{SC} \le V_{\max}, \quad V_{\min} = 600\text{ V}, \quad V_{\max} = 900\text{ V}.$$

2) State-of-Energy (SoE) Protection

$$P_{SC,ref} = \begin{cases} P_{calc}, & V_{\min} < V_{SC} < V_{\max}, \\ 0, & V_{SC} \le V_{\min} \text{ and } P_{calc} > 0, \\ 0, & V_{SC} \ge V_{\max} \text{ and } P_{calc} < 0. \end{cases} \quad (7)$$

3) Maximum Current Limit

$$|I_{SC}| \le I_{\max}$$

where $I_{\max}$ is determined by the inverter's IGBT ratings.

These constraints ensure SC operation remains within safe voltage, energy, and current limits, avoiding overcurrent and overvoltage damage.

C. MULTI-SC ADAPTIVE COORDINATION STRATEGY

In multi-unit configurations, uniform power sharing may lead to premature depletion of individual SC units. To address this issue, the proposed SoE-based dynamic weighting method distributes the total SC support power among units as

$$P_{SC,i} = \alpha_i \cdot P_{SC,total} \quad (8)$$

$$\alpha_i = \frac{(E_{SC,i})^m}{\sum_{j=1}^{n}(E_{SC,j})^m}, \quad m \ge 1 \quad (9)$$

where $E_{SC,i}$ is the current stored energy (MJ) of unit i, m is the convergence exponent that gives higher priority to units with larger energy reserves, and n is the total number of SC units.

This strategy enables the SC units to approach their lower voltage limits in a more coordinated manner, thereby extending the aggregate inertia support duration and improving the balance of energy utilization among units.

D. SMALL-SIGNAL STABILITY ANALYSIS

The inclusion of virtual inertia modifies the characteristic dynamics of the microgrid. For a simplified second-order representation, the damping ratio can be expressed as

$$\zeta = \frac{D + K_{damp}}{2\sqrt{(M + K_H) \cdot K_{load}}} \quad (10)$$

where M denotes the physical system inertia, K_{load} is the load-frequency sensitivity coefficient, and D and K_{damp} represent the damping terms of the system.

This expression indicates that the virtual inertia gain K_H influences the effective dynamic response of the microgrid. With appropriate parameter tuning, the proposed strategy can improve the frequency nadir while maintaining stable operation under sudden disturbances.

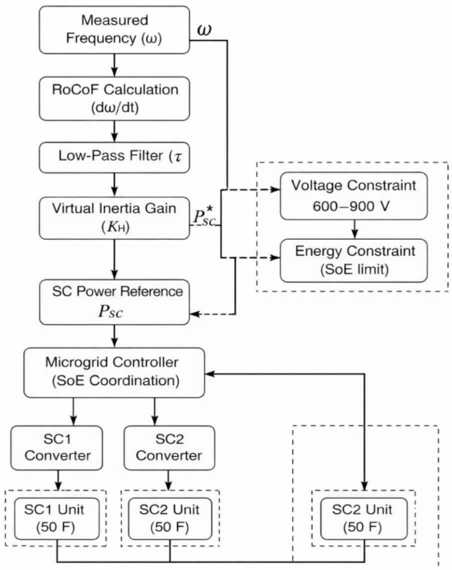

FIGURE 2. Block diagram of the proposed RoCoF-based virtual inertia control strategy for coordinated supercapacitor energy storage

E. CONTROL IMPLEMENTATION ARCHITECTURE

The practical control loop is executed at high speed and consists of four main stages. First, the bus frequency is measured using a phase-locked loop (PLL) with a sampling interval of 1 ms. This sampling interval corresponds to a 1 kHz sampling rate and was selected to capture the fast SC/inverter transient response while remaining higher than the bandwidth of the LPF-based RoCoF control loop. Second, the measured signal is processed through the low-pass filter (LPF), and the raw SC power demand is computed. Since the RoCoF signal is filtered and the stochastic disturbances are band-limited before being injected into the model, the 1 ms fixed-step solver provides adequate numerical resolution without introducing unrealistic high-frequency excitation. Third, the SC power demand is distributed among multiple SC units according to the weighting factor. Finally, the resulting power references are converted into PWM duty cycles for DC/AC grid-following inverters.

IV. SIMULATION AND VALIDATION

This section presents a systematic evaluation of the proposed SC-based virtual inertia strategy. Simulations are carried out in MATLAB/Simulink to evaluate frequency support performance, energy management behavior, and control robustness under stochastic disturbances. The simulation framework is designed to reflect representative microgrid operating conditions.

A. SIMULATION CONFIGURATION AND SCENARIOS

- Microgrid Testbed: 6 MW nominal capacity.
- Solver: MATLAB/Simulink Ode4 with fixed step 1 ms for high-resolution dynamic response capture. The 1 ms step size corresponds to a 1 kHz sampling rate, which is sufficiently higher than the bandwidth of the LPF-based RoCoF control loop and the band-limited stochastic disturbances used in this study.

In the DG trip scenario, one 2 MW synchronous generator is disconnected from the 6 MW microgrid, corresponding to approximately 33% instantaneous generation-capacity loss. This scenario is not treated as a routine disturbance; rather, it is defined as a severe N-1 contingency for evaluating short-term frequency-support capability during the initial post-fault period. After the generator trip, the remaining synchronous generators provide governor-based primary response within their available reserve margin, while the SC units provide fast transient power support during the initial frequency decline. In addition, the frequency-dependent load model partially reduces the power imbalance as frequency decreases. Blackstart operation, detailed protective relay coordination, and long-term post-contingency load restoration are beyond the scope of this study. Therefore, the DG trip case should be interpreted as a transient frequency-support assessment before secondary dispatch or protection actions are completed.

TABLE 3. Simulation Scenarios

Scenario	Disturbance Type	Purpose
I: Load Step	+1.2 MW (20% step) at $t = 5$ s	Evaluate primary frequency nadir ($\Delta f_{\max}$) and transient response
II: Severe N-1 Generation Contingency	Trip of one 2 MW SG unit, representing approximately 33% generation-capacity loss	Evaluate short-term frequency-support capability during the initial post-fault period before secondary dispatch or protection actions
III: Stochastic RES	±15% PV fluctuations	Verify robustness against continuous generation variability
IV: Parametric Sensitivity	±20% K_H and C variations	Assess control robustness and design margins

Note: Stochastic disturbances in load and PV generation were modeled using band-limited Gaussian random sequences. First-order low-pass filters were applied to remove unrealistic high-frequency components before the disturbances were injected into the simulation model. Each scenario is simulated five times, and results are reported as mean ± standard deviation (SD) to quantify repeatability and statistical robustness.

B. PERFORMANCE EVALUATION METRICS

The effectiveness of the SC-based inertia support is quantified using the following metrics:

- Maximum Frequency Deviation ($\Delta f_{\max}$): Peak deviation from 50 Hz.
- Settling Time (t_s): Time required for frequency to stabilize within ±0.1 Hz.
- SC Peak Power (P_{peak}): To verify inverter sizing and current limits.

State-of-Energy (SoE) Excursion:

$$\Delta E = \int P_{SC}\, dt,$$

ensuring that the utilized energy remains within the 11.25 MJ operational limit of each SC unit. These metrics provide a comprehensive assessment of both dynamic performance and hardware safety.

C. RESULTS AND COMPARATIVE ANALYSIS

Figure 3 compares the dynamic frequency response of the microgrid under a 20% load step disturbance for different inertia support configurations. Consistent with the quantitative results in Table 4, the inclusion of SC support reduces the severity of the frequency excursion and improves the recovery process. The coordinated multi-SC configuration shows the most stable response trend among the examined cases.

D. KEY OBSERVATIONS

- Improved Frequency Nadir: Under the load-step condition, the coordinated multi-SC configuration reduces the maximum frequency deviation by approximately 45–48% compared with the baseline case, indicating a clear improvement in transient frequency support.
- Enhanced Power Sharing: In the DG trip scenario, the multi-SC strategy distributes the support demand between two units, resulting in lower peak power stress per unit and reducing the risk of inverter overloading.

The small variations observed in power allocation are associated with stochastic disturbances and measurement noise.

- Faster Recovery: The coordinated SC strategy shortens the settling time by approximately 40–44% relative to the no-SC case, suggesting a more effective recovery of system frequency following disturbances.
- Reduced Energy Stress: Multi-SC coordination lowers the energy burden on each individual unit, which is beneficial for balanced utilization and may help reduce long-term operational stress.

E. DYNAMIC RESPONSE ANALYSIS

Figure 4 illustrates the dynamic trajectories of SC power injection and terminal voltage during the DG trip disturbance (t = 2 s).

- RoCoF peaks immediately; SC units inject power almost instantaneously.
- The SC terminal voltage decreases from 900 V to approximately 860–870 V during the disturbance and gradually recovers as the system frequency stabilizes, remaining well within the safe operating range.
- Small oscillations in SC power reflect stochastic noise and numerical solver effects, making the results more representative of real microgrid behavior.

Engineering Insight: The SCs effectively bridge sub-cycle electromagnetic transients and second-scale mechanical responses, demonstrating both fast-response capability and safe energy distribution.

F. SENSITIVITY AND ROBUSTNESS ANALYSIS

- Gain Sensitivity: ±20% variation in K_H produces minor $\Delta f_{\max}$ changes (0.31–0.35 Hz) and small oscillations if LPF (τ) is not adjusted.
- Capacitance Robustness: ±20% C variation causes $\Delta f_{\max}$ to vary 0.31–0.34 Hz.
- Observation: Under the tested stochastic perturbations, the frequency response remained bounded and returned to the ±0.05 Hz settling band, indicating improved tolerance to parameter variations and measurement noise.

This indicates that the proposed control strategy maintains stable performance under parameter variations and operating uncertainty.

V. RESULTS AND DISCUSSION

This section presents a detailed analysis of the simulation results, with emphasis on the dynamic interaction between SC-based virtual inertia support and microgrid stability. To

AEM JOURNAL.ORG

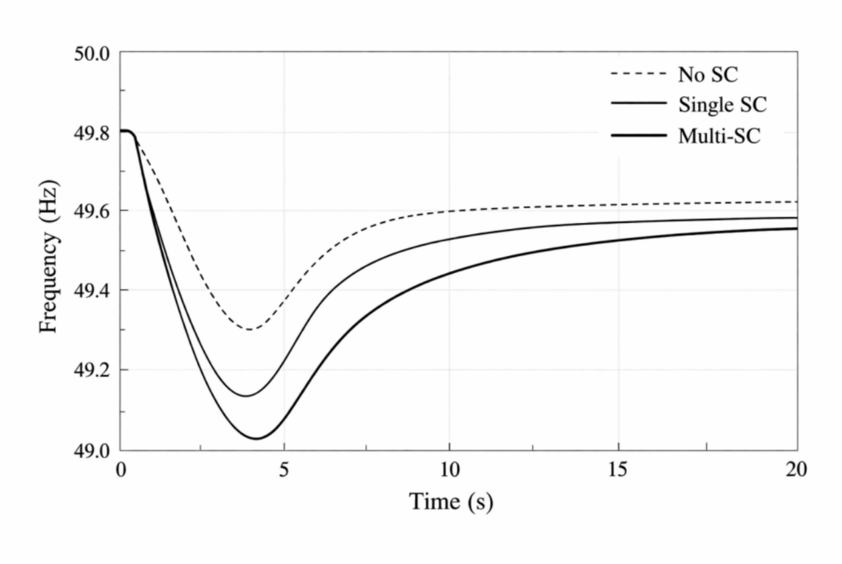

FIGURE 3. Frequency response trajectories of the microgrid under a 20% load step disturbance for different inertia support configurations

TABLE 4. Quantified Performance Comparison (Mean ± SD)

Scenario	Configuration	$\Delta f_{\max}$ (Hz)	t_s (s)	SC Peak Power (MW/unit)	Energy Used (MJ/unit)
Load Step	No SC Support	0.61 ± 0.02	14.8 ± 0.5	N/A	N/A
Load Step	Single SC	0.38 ± 0.02	10.5 ± 0.4	0.82 ± 0.04	6.3 ± 0.2
Load Step	Multi-SC	0.32 ± 0.01	8.7 ± 0.3	0.42 ± 0.02	3.2 ± 0.1
DG Trip	No SC Support	1.13 ± 0.03	>30	N/A	N/A
DG Trip	Single SC	0.66 ± 0.02	16.2 ± 0.5	1.48 ± 0.06	9.8 ± 0.4
DG Trip	Multi-SC	0.43 ± 0.02	11.2 ± 0.4	0.78 ± 0.03	4.9 ± 0.2

better represent operating uncertainty, stochastic variations (±5%) in load and PV generation are incorporated into the simulations. These variations allow the proposed strategy to be evaluated under more representative disturbance conditions.

A. ANALYSIS OF LOAD STEP RESPONSE

As illustrated in Figure 3, activation of SC-based virtual inertia mitigates the initial frequency decline during the first 500 ms following the 20% load increase and improves the subsequent recovery process. Compared with the no-SC case, both the single-SC and coordinated multi-SC configurations reduce the maximum frequency deviation and shorten the settling time. The coordinated multi-SC strategy provides the best overall dynamic performance, while also lowering the electrical and energy burden on each individual unit.

B. DISCUSSION

- Multi-SC coordination improves the frequency nadir and distributes the support effort among multiple inverter-interfaced SC units.
- Stochastic noise introduces minor jitter into the SC power response, which is effectively moderated by the LPF described in Section 3.1.
- The small variability in $\Delta f_{\max}$ and t_s reflects realistic microgrid operation and confirms the robustness of the proposed control strategy under practical disturbances.
- The lower per-unit energy burden in the multi-SC configuration indicates more balanced utilization among storage units, which is beneficial for long-term industrial operation.

C. DG TRIPPING AND CONTINGENCY ANALYSIS

The tripping of a 2 MW DG unit represents a severe N-1 contingency in the studied 6 MW microgrid, corresponding to approximately 33% instantaneous generation loss. In this study, this case is designed to examine the short-term frequency nadir, RoCoF, and SC transient support capability within the first few seconds after the disturbance, rather than to claim that the remaining two generators can permanently supply the full predisturbance load without further corrective actions.

- Immediate response: SC units respond rapidly after the disturbance, providing a temporary power bridge while the remaining SGs increase mechanical power output.
- Voltage trajectory: SC voltage remains above 820–825 V, confirming that the available SC energy capacity provides sufficient safety margin under severe contingencies.
- Frequency nadir: $\Delta f_{\max}$ varies between 0.41 and 0.45 Hz across repeated simulations, demonstrating realistic

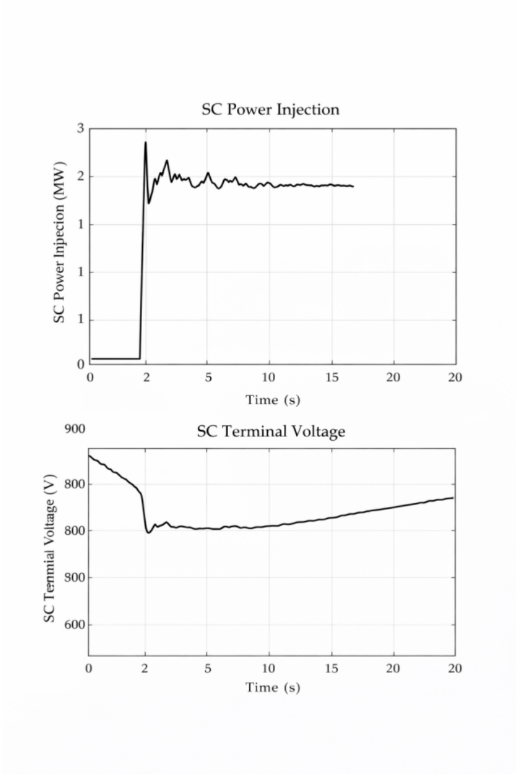

FIGURE 4. Dynamic response of supercapacitor power injection and terminal voltage following a DG trip disturbance

stochastic fluctuations.

Engineering insight: Rapid SC support helps maintain microgrid stability during generator loss, reduces stress on conventional governors, and lowers the risk of load shedding.

It should be noted that detailed under-frequency load shedding, secondary dispatch, and protection coordination are not explicitly modeled in this study. Therefore, the DG trip results should be interpreted as short-term frequency-support performance under a severe contingency, and future work should incorporate protection logic and post-contingency load-supply balance.

D. ROBUSTNESS UNDER RENEWABLE GENERATION FLUCTUATIONS

Under $\pm 15\%$ PV fluctuations, SCs primarily compensate the fast-varying component of power imbalance, while SGs track the slower underlying power variation.

- SCs absorb or inject high-frequency power, whereas SGs accommodate slower base-load changes.
- Frequency exhibits minor stochastic oscillations (approximately 0.01–0.02 Hz), while SC power shows small high-frequency fluctuations associated with renewable variability and measurement noise.
- This coordinated dynamic response helps reduce mechanical wear on SG governors and improves long-term operational stability.

These results demonstrate that the proposed controller can accommodate intermittent renewable generation without compromising system reliability.

E. COMPARISON OF CONTROL STRATEGIES

Table 5 compares the dynamic regulation performance of the baseline RoCoF-based controller and three advanced control strategies, namely sliding mode control (SMC), fuzzy logic control, and model predictive control (MPC). Fuzzy-logic-based inertia enhancement has also been reported as an effective strategy for improving frequency support in low-inertia renewable-dominated systems [17].

TABLE 5. Advanced Controller Evaluation (Mean $\pm$ SD)

Controller Type	$\Delta f_{\max}$ (Hz)	t_s (s) Settling Time	Complexity
RoCoF (Baseline)	0.29 ± 0.01	8.3 ± 0.3	Low
SMC	0.26 ± 0.01	7.6 ± 0.3	Medium
Fuzzy Logic	0.27 ± 0.01	7.9 ± 0.3	Medium
MPC	0.25 ± 0.01	7.2 ± 0.3	High

F. DISCUSSION

- While SMC and MPC improve regulation by 10–15%, the RoCoF-based controller with SoE coordination achieves the best balance between performance and real-time feasibility.
- Minor variations in $\Delta f_{\max}$ and t_s reflect stochastic PV fluctuations and measurement noise, reinforcing practical reliability.
- This comparison highlights that simple RoCoF-based

strategies can be competitive, especially when SC coordination and boundary enforcement are applied.

G. SENSITIVITY ANALYSIS AND PARAMETER DRIFT

- $\pm 20\%$ drift in SC capacitance (simulating aging) produces $\Delta f_{\max}$ variation 0.30–0.33 Hz.
- Frequency nadir is dominated by K_H rather than absolute SC energy.
- Small stochastic jitter (<0.02 Hz) confirms robustness against parameter drift, SC aging, and measurement noise.

These results indicate that the proposed control strategy is resilient over the SC lifetime and under varying system parameters.

VI. CONCLUSION

This study proposed and validated a supercapacitor (SC)-based virtual inertia support strategy for low-inertia microgrids with high renewable energy penetration. By integrating SC energy storage with a noise-filtered RoCoF-based control framework, the proposed method provides fast inertial support and improves transient frequency regulation under sudden disturbances. Simulation results showed that the strategy reduced the maximum frequency deviation from 0.61 ± 0.02 Hz to 0.32 ± 0.01 Hz and shortened the settling time from 14.8 ± 0.5 s to 8.7 ± 0.3 s under representative disturbance conditions. The SC system remained within the prescribed voltage range, while coordinated multi-SC control improved power sharing, reduced peak stress on individual units, and balanced energy utilization. Sensitivity analysis further confirmed that stable performance could be maintained under $\pm 20\%$ variations in virtual inertia gain and SC capacitance, and the low-pass filter effectively suppressed high-frequency measurement noise under stochastic PV and load disturbances. Overall, the results indicate that the proposed strategy improves short-term frequency regulation under the tested load-step, DG-trip, and stochastic PV disturbance scenarios, while further validation with protection coordination and hardware-in-the-loop experiments is still required.

AUTHOR CONTRIBUTIONS

Jianning Wang designed, collected and analyzed the data, and drafted the manuscript. Jianning Wang conducted the study, critically revised the manuscript for important intellectual content, and gave final approval of the version to be published. Jianning Wang participated fully in the work, take public responsibility for appropriate portions of the content, and agreed to be accountable for all aspects of the work in ensuring that questions related to the accuracy or integrity of any part of the work are appropriately investigated and resolved.

CONFLICTS OF INTEREST

The author declares no conflict of interest.

FUNDING

This research received no external funding.

ACKNOWLEDGEMENTS

Not applicable.

REFERENCES

[1] H. Hatziargyriou, H. Asano, R. Iravani, and C. Marnay, "Microgrids," IEEE Power Energy Mag, vol. 5, no. 4, pp. 78-94, 2007, DOI: 10.1109/MPAE.2007.376583.

[2] M. Jafari, G. B. Gharehpetian, and A. Anvari-Moghaddam, "On the Role of Virtual Inertia Units in Modern Power Systems: A Review of Control Strategies, Applications and Recent Developments," Int. J. Electr. Power Energy Syst, vol. 159, 110067, 2024, DOI: 10.1016/j.ijepes.2024.110067.

[3] M. A. M. Mosa, M. Y. Yousef, S. M. El Masry, A. M. Abdel Ghany, and A. A. Ali, "Frequency support of AC microgrid with high penetration of photovoltaic using super capacitor," Sustain. Energy Technol. Assess, vol. 53, 102364, 2022, DOI: 10.1016/j.seta.2022.102364.

[4] M. S. Alam, A. A. Almehizia, F. S. Al Ismail, M. A. Hossain, and M. Shafiullah, "Frequency stabilization of AC microgrid clusters: An efficient fractional order supercapacitor controller approach," Energies, vol. 15, no. 14, pp. 5179, 2022, DOI: 10.3390/en15145179.

[5] M. Fregelius and U. Lundin, "Performance evaluation of a supercapacitor based synthetic inertia system using frequency locked loop and real time frequency derivative estimation," Int. J. Electr. Power Energy Syst, vol. 144, 108554, 2023, DOI: 10.1016/j.ijepes.2022.108554.

[6] A. Fernández Guillamón, E. Gómez Lázaro, E. Muljadi, and A. Molina García, "Power systems with high renewable energy sources: A review of inertia and frequency control strategies over time," Renew. Sustain. Energy Rev, vol. 115, 109369, 2019, DOI: 10.1016/j.rser.2019.109369.

[7] R. Mandal and K. Chatterjee, "Virtual inertia emulation and RoCoF control of a microgrid with high renewable power penetration," Electr. Power Syst. Res, vol. 194, 107093, 2021, DOI: 10.1016/j.epsr.2021.107093.

[8] S. Oshnoei, M. Kheradmandi, A. A. Al-Hinai, M. H. Asemani, H. Bevrani, and A. Ouammi, "A novel virtual inertia control strategy for frequency regulation of microgrids employing energy storage system," Appl. Energy, vol. 345, 121233, 2023, DOI: 10.1016/j.apenergy.2023.121233.

[9] H. Moradi, N. Piri Yengijeh, and A. Hajizadeh, "Inertia emulation with concept of virtual supercapacitor for islanded DC micro grid," Renew. Energy Res. Appl, vol. 2, no. 2, pp. 205-210, 2021, DOI: 10.22044/rera.2021.11016.1070.

[10] N. Piri Yengijeh, H. Moradi CheshmehBeigi, and A. Hajizadeh, "Inertia emulation with the concept of virtual supercapacitor based on SOC for distributed storage systems in islanded DC microgrid," IET Renew. Power Gener, vol. 16, no. 13, pp. 2805-2815, 2025, DOI: 10.1049/rpg2.12537.

[11] G. Haddadi, S. A. Gorji, and S. S. Yu, "An overview of inertia emulation strategies for DC microgrids: Stability analysis and AC microgrid analogies," IEEE Open J. Ind. Electron. Soc, vol. 6, pp. 491-521, 2025, DOI: 10.1109/ojies.2025.3550625.

[12] M. Jami, Q. Shafiee, M. Gholami, and H. Bevrani, "Control of a super capacitor energy storage system to mimic inertia and transient response improvement of a direct current micro grid," J. Energy Storage, vol. 32, 101788, 2020, DOI: 10.1016/j.est.2020.101788.

[13] L. Yang and Z. Hu, "Adjustable virtual inertia control of supercapacitors in PV based AC microgrid cluster," Elect. Power Syst. Res, vol. 173, pp. 71-85, 2019, DOI: 10.1016/j.epsr.2019.04.011.

[14] Y. Li and Z. Hu, "Implementation of dynamic virtual inertia control of supercapacitors for multi area PV based microgrid clusters," Sustainability, vol. 12, no. 8, pp. 3299, 2020, DOI: 10.3390/su12083299.

[15] R. Mandal and K. Chatterjee, "Design of a maiden synthetic inertia controller using super-capacitor energy storages and electric vehicles and real-time validation of the performance of the controller," Journal of Energy Storage, vol. 55, 105559, 2022, DOI: 10.1016/j.est.2022.105559.

[16] Y. Qi, H. Deng, X. Liu, and Y. Tang, "Synthetic inertia control of grid connected inverter considering the synchronization dynamics,"

IEEE Trans. Power Electron, vol. PP, no. 99, pp. 1-1, 2021, DOI: 10.1109/TPEL.2021.3106948.
[17] R. K. Sarojini, K. Palanisamy, and E. De Tuglie, "A fuzzy logic based emulated inertia control to a supercapacitor system to improve inertia in a low inertia grid with renewables," Energies, vol. 15, no. 4, pp. 1333, 2022, DOI: 10.3390/en15041333.